Nanoscale-SiC doping for enhancing J_c and H_{c2} in superconducting MgB_2

S. X. Dou[a)]
Institute for Superconducting and Electronic Materials, University of Wollongong, Wollongong, New South Wales 2522, Australia

V. Braccini
Applied Superconductivity Center, University of Wisconsin–Madison, Wisconsin 53706 and Applied Conductivity Centre, University of Wisconsin-Madison, Madison, Wisconsin 53706

S. Soltanian
Institute for Superconducting and Electronic Materials, University of Wollongong, Wollongong, New South Wales 2522, Australia

R. Klie and Y. Zhu
Brookhaven National Laboratory, Utpn, New York 11973

S. Li
Advanced Materials Research Center, Nanyang Technological University, 639798, Singapore

X. L. Wang
Institute for Superconducting and Electronic Materials, University of Wollongong, Wollongong, New South Wales 2522, Australia

D. Larbalestier
Applied Superconductivity Center, University of Wisconsin-Madison, Wisconsin 53706 and Applied Conductivity Centre, University of Wisconsin-Madison, Madison, Wisconsin 53706

(Received 30 January 2004; accepted 16 September 2004)

The effect of nanoscale-SiC doping of MgB_2 was investigated in comparison with undoped, clean-limit, and Mg-vapor-exposed samples using transport and magnetic measurements. It was found that there are two distinguishable but related mechanisms that control the critical current-density-field $J_c(H)$ behavior: increase of upper critical field H_{c2} and improvement of flux pinning. There is a clear correlation between the critical temperature T_c, the resistivity ρ, the residual resistivity ratio RRR$=R(300\ \mathrm{K})/R(40\ \mathrm{K})$, the irreversibility field H^*, and the alloying state in the samples. The H_{c2} is about the same within the measured field range for both the Mg-vapor-treated and the SiC-doped samples. However, the $J_c(H)$ for the latter is higher than the former in a high-field regime by an order of magnitude. Mg vapor treatment induced intrinsic scattering and contributed to an increase in H_{c2}. SiC doping, on the other hand, introduced many nanoscale precipitates and disorder at B and Mg sites, provoking an increase of $\rho(40\ \mathrm{K})$ from 1 $\mu\Omega$ cm (RRR$=15$) for the clean-limit sample to 300 $\mu\Omega$ cm (RRR$=1.75$) for the SiC-doped sample, leading to significant enhancement of both H_{c2} and H^* with only a minor effect on T_c. Electron energy-loss spectroscope and transmission electron microscope analysis revealed impurity phases: Mg_2Si, MgO, MgB_4, BO_x, $Si_xB_yO_z$, and BC at a scale below 10 nm and an extensive domain structure of 2–4-nm domains in the doped sample, which serve as strong pinning centers. © *2004 American Institute of Physics*. [DOI: 10.1063/1.1814415]

INTRODUCTION

The critical current density J_c in MgB_2 has been a central topic for extensive research efforts since superconductivity in this compound was discovered.[1] A number of techniques have been developed and employed to improve the J_c performance in magnetic fields. By using nanoparticle SiC doping of MgB_2, we have achieved a J_c enhancement in high fields of more than one order of magnitude, with only a slight reduction in T_c.[2] It was proposed that a high density of nanoinclusions and a possible substitution of SiC for B in MgB_2 was responsible for enhancing $J_c(H)$ over a wide range of temperatures.

Recently, using high-field transport measurements, Gurevich *et al.* have reported the achievement of record-high upper critical fields H_{c2} for high-resistivity films and untextured bulk polycrystals.[3] They found that enhancements to the resistivity have a strong influence on H_{c2}. The observed remarkable H_{c2} enhancement to almost 50 T is a consequence of the two-gap superconductivity of MgB_2,[3] which offers special opportunities for further H_{c2} increase by tuning the impurity scattering. Nanoscale-SiC doping introduces a large degree of alloying and greatly raises resistivity, too. Thus, we expected that transport measurements on SiC-doped samples would provide additional useful information for understanding the pinning mechanisms and H_{c2} behavior of alloyed MgB_2. In this paper, we report on such transport and magnetic measurement evaluations in combination with

[a)]Electronic mail: shi_dou@uow.edu.au

transmission electron microscope (TEM) observations on the nanoscale-SiC-doped MgB_2. A set of four samples ranging from the clean limit to very dirty state have wild variation of normal-state resistivity from 1 to 300 $\mu\Omega$ cm and significantly different electromagnetic properties which allow us to understand the mechanisms behind the enhancement of $J_c(H)$.

EXPERIMENTAL DETAILS

MgB_2 pellet samples were prepared by an *in situ* reaction method, described in detail previously.[2] Powders of magnesium (99%) and amorphous boron (99%) were well mixed with SiC nanoparticle powder (size: 10–100 nm) with the atomic ratio of MgB_2 and with 10 wt % (sample B) and 0 wt % (sample A) SiC addition. Pellets 10 mm in diameter and 2 mm in thickness made under a uniaxial pressure were sealed in an Fe tube and then heated at 800 °C for 30 min in flowing high-purity Ar, followed by furnace cooling to room temperature. These two Wollongong samples were compared to two Madison samples, one being the clean limit (sample C) and the second being the same sample exposed to Mg vapor (sample D), as described in detail elsewhere.[4]

The resistivity versus temperature curves, $\rho(T)$, were measured in magnetic fields up to 9 T by a four-probe method at a current density of about 1 A/cm^2 using a 9-T Physical Property Measurement System (Quantum Design). From the resistivity curves, we defined the upper critical field as $R(H_{c2})=0.9\,R(T_c)$. Magnetization was measured from 5 to 30 K using an Oxford 14-T vibrating sample magnetometer (VSM). Bar-shaped samples of about the same size were cut from the as-sintered pellets to minimize size-dependent effects.[5] Magnetic J_c values were determined from the magnetization hysteresis loops using the appropriate critical state model.[6] An empirical magnetic irreversibility line, H_M^*, was defined as the field at which J_c falls to 100 A/cm^2.[4] High-resolution transmission electron microscopy was employed to characterize the morphology of the samples. Electron energy-loss spectroscopy[7] (EELS) was obtained using a JEOL-3000F field-emission scanning transmission electron microscope TEM, equipped with a Schottky field-emission source operated at 300 keV.

RESULTS

Figure 1 shows the resistivity curves, $\rho(T)$, up to 9 T for the undoped (a) and the SiC-doped (b) samples. The onset T_c of the undoped sample was 37.5 K. For the 10 wt % SiC-doped sample, T_c decreased only by 0.6 K. By contrast, T_c is depressed to about 22 K for C-doped MgB_2 with a nominal stoichiometry of $Mg(B_{0.8}C_{0.2})_2$ synthesized from Mg and B_4C.[8] This indicates that the proportion of C added SiC to substitute for B in the lattice is small compared to the pure C substitution case. The majority of SiC ends up with various impurity phases at nanoscale, as evidenced by the EELS analyses. It is noted that the $\rho(T)$ curves for the doped sample shifted with increasing field much more slowly than the undoped one, as is shown explicitly in Fig. 2, where the H_{c2} obtained from the 90% values of the resistive transitions from Fig. 1 are shown. It is also noted that the $\rho(T)$ curve for

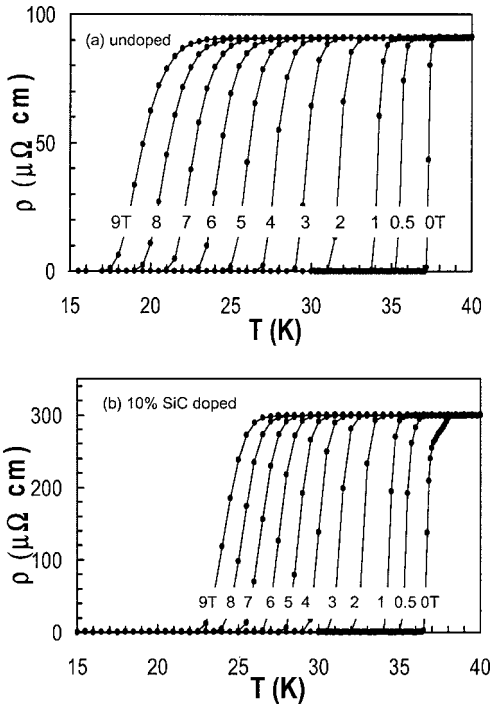

FIG. 1. The resistivity vs temperature in fields up to 9 T for the undoped (a) and SiC-doped (b) samples.

the doped sample in self-field showed a special feature of two-step transition. This is due to the inhomogeneity of this sample because the 10% SiC addition resulted in a number of impurity phases coexisting with MgB_2. This will be further confirmed in EELS analyses in a later section. A further important point is that the nominal resistivities of the two samples are very different, $\rho(40\text{ K})$ being 90 $\mu\Omega$ cm for the undoped sample and 300 $\mu\Omega$ cm for the doped sample. We consider that the 90% transition approximates H_{c2}. Figure 2 also includes the same data taken on the clean-limit [$\rho(40\text{ K})=1$ $\mu\Omega$ cm] and Mg-exposed sample [$\rho(40\text{ K})=18$ $\mu\Omega$ cm] of Braccini *et al.*[4] It is interesting to note that the Mg-exposed sample has the highest H_{c2}, then the SiC doped, undoped, and the clean limit. Figure 3 shows a typical example of the half $M-H$ loop at 20 K for the undoped sample (A) and 10% SiC-doped-MgB_2 sample (B). It is clear that the closing field of the $M-H$ loop for the sample B is

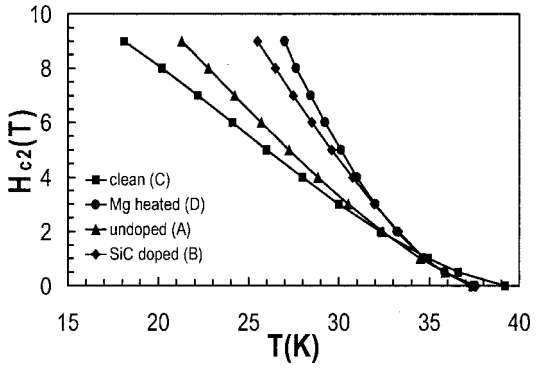

FIG. 2. The 90% of the resistive transition (upper critical field) as a function of the temperature for the undoped (A), the 10 wt % SiC-doped (B), the clean-limit, (C) and the Mg-vapor-treated (D) samples.

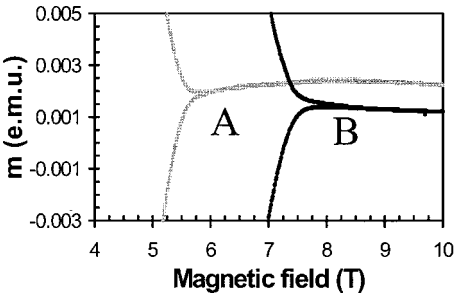

FIG. 3. The M–H loop at 20 K for the undoped sample (A) and the SiC-doped sample (B).

2 T higher than that for the sample A. The magnetic J_c for all the samples was calculated from the $M-H$ loops at 4.2, 10, 20, and 30 K. Figure 4 shows the magnetic J_c vs H for the four samples at 4.2 and 20 K. Consistent with its higher H_{c2}, the doped sample shows a smaller dependence of J_c on magnetic field at all temperatures. At 4.2 K and low field, both the SiC-doped and undoped samples attain about 10^5 A/cm^2 while falling to 100 A/cm^2 at 7.4 and 5.6 T at 20 K, respectively. The J_c values for the Wollongong samples (A and B) are much higher than for the two Madison samples (C and D). At 20 K, the 10 wt % SiC-doped sample achieved 10^5 A/cm^2 at 3 T, comparable to that of state-of-the-art Ag/Bi-2223 tapes, and an order of magnitude higher than recent state-of-the-art Fe/MgB_2 tapes.[9] These results significantly strengthen the position of MgB_2 as a competitor for both low- and high-temperature superconductors.

The irreversibility fields (H_M^*), derived from the fields at which the magnetic hysteresis loops obtained with the VSM indicate that $J_c = 100$ A/cm^2, are shown in Fig. 5. Doping with SiC significantly improved H_M^*. Here, in contrast to the H_{c2}, we note that the SiC-doped sample has the best H_M^* at all temperatures while the Mg-exposed sample has H_M^* even lower than the undoped at high temperatures but crosses over the undoped at low temperatures. For example, H_M^* for the

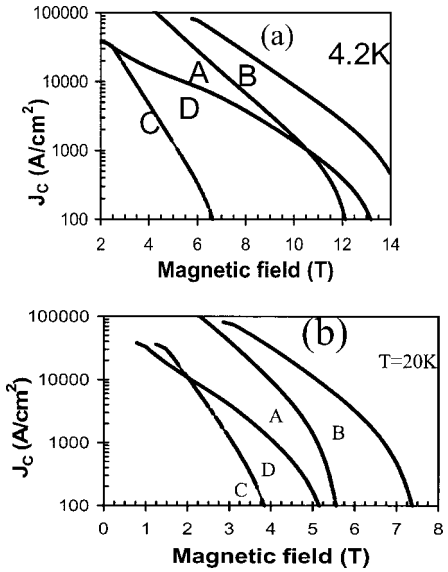

FIG. 4. A comparison of $J_c(H)$ for the undoped (A), 10 wt % SiC-doped (B), the clean-limit (C), and the Mg-vapor-treated (D) samples at 4.2 K (a) and 20 K (b).

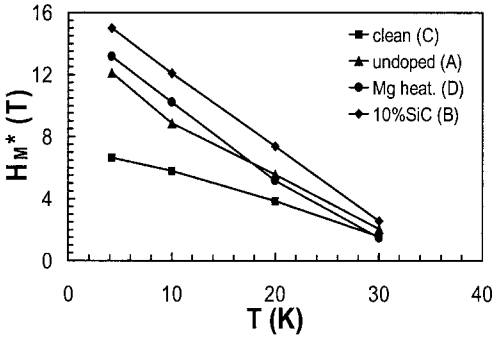

FIG. 5. The irreversibility field H_M^* vs temperature for the samples A, B, C, and D.

SiC-doped sample reached 7.4 T, compared to 5.6 T for the undoped one, 5.2 T for the Mg-vapor-treated one, and 3.8 T for the clean-limit one at 20 K.

The TEM examination revealed that there are a number of impurity phases in the form of nanometer-size inclusions inside and in between grains in the nano-SiC-doped sample. These impurities include Mg_2Si, MgB_4, and MgO detected by x-ray diffraction (XRD) analysis[2,10] and unreacted SiC, amorphous BO_x, $Si_xB_yO_z$, and BC detected by using the EELS technique. TEM images show that the grain size of MgB_2 is smaller than 100 nm. Energy dispersive x-ray (EDX) analysis shows that the Mg:Si ratio is identical across the entire sample, indicating that the phase distribution is globally homogeneous. However, the nanoscale impurity phases MgB_4 and MgO are present within the grains. The presence of oxygen within grains is consistent with the results obtained from the above-mentioned 220-$\mu\Omega$ cm thin film with strong pinning, where the ratio of Mg:B:O reached 1.0:0.9:07.[11] Figure 6 is a TEM image showing some unreacted SiC particles and a corresponding lattice image. The EELS analysis [convergence angle $(\alpha) = 13$ mrad and collection angle $(\theta_c) = 18$ mrad] shows that this particle is indeed pure SiC without B or any other element in it. The EELS analyses also show other phases present in the SiC-doped sample. Figure 7(a) shows the EELS spectrum of the $Si_xB_yO_z$ phase with no C. The fine structure of both Si and B suggests that the phase is amorphous. Figure 7(b) is the EELS spectrum of the BC phase. Again, the fine structure of B suggests that the phase is amorphous. The EELS of amorphous BO_x is shown in Fig. 7(c). These phases are often seen in the close vicinity of MgB_2 grains in the sample.

Based on lattice-parameter changes and EDX analysis, we suggested that C and Si might substitute into the lattice in an earlier work.[2] However, in a recent work on SiC-doped MgB_2, single crystal grown under high pressure (30 kbar) and high temperature (1900–1950 °C) showed there was only C substitution for B but no Si detected in the crystals. The authors revealed that the C substitution for B was as high as 16%, the highest level of substitution in all the C-doping studies so far.[12] There is a clear trend with respect to C substitution in MgB_2 in the literature data.[13–16] The higher the sintering temperature is, the larger the proportion of C that is substituted for B in MgB_2. As we used relatively low sintering temperatures, 800–850 °C, the C substitution for B is expected to be lower. Figure 8(a) is the *Z*-contrast

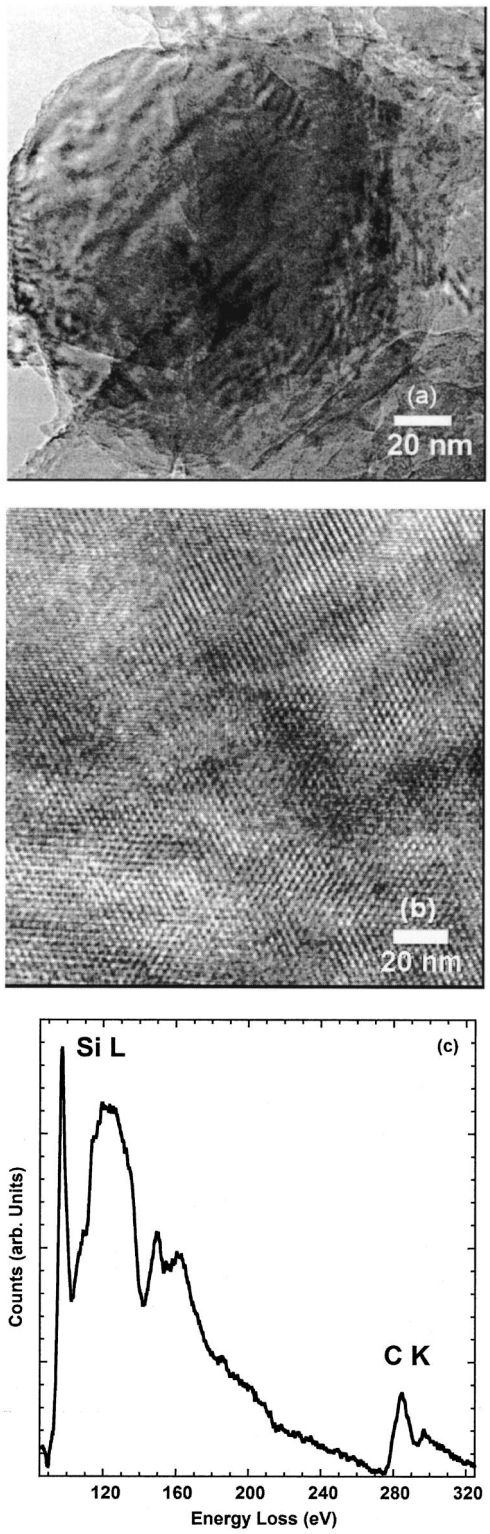

FIG. 6. Conventional TEM image of an unreacted SiC particle, (b) high-resolution TEM image of the bulk of the SiC particle, and (c) EELS spectrum clearly showing the Si L- and the C K-edge.

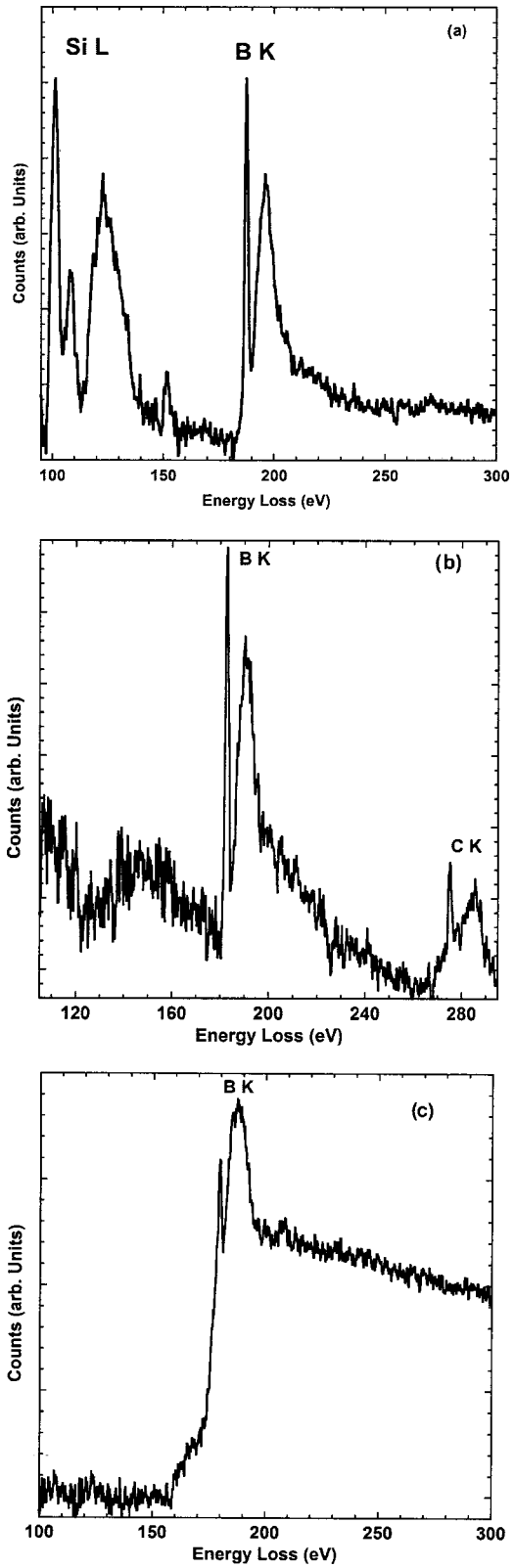

FIG. 7. The EELS spectrum of amorphous (a) $Si_xB_yO_z$, (b) BC, and (c) BO_x detected in the SiC-doped MgB_2.

image[17–19] for the nano-SiC-doped sample, which shows a typical MgB_2 crystal in the [100] orientation. *Z*-contrast imaging in scanning transmission electron microscopy mode utilizes electrons scattered at high angle (>25 mrad) to form an incoherent image, with an image intensity that is proportional to the square of the average atomic number (i.e., $\sim Z^2$). A close-up look at the atomic structure of the high-resolution lattice image shows that only the Mg columns are visible [Fig. 8(b)], due to the small scattering amplitude of B. The EELS shows the typical fine structure for B in MgB_2,[20] but no C signal can be detected [Fig. 8(c)]. It should be noted

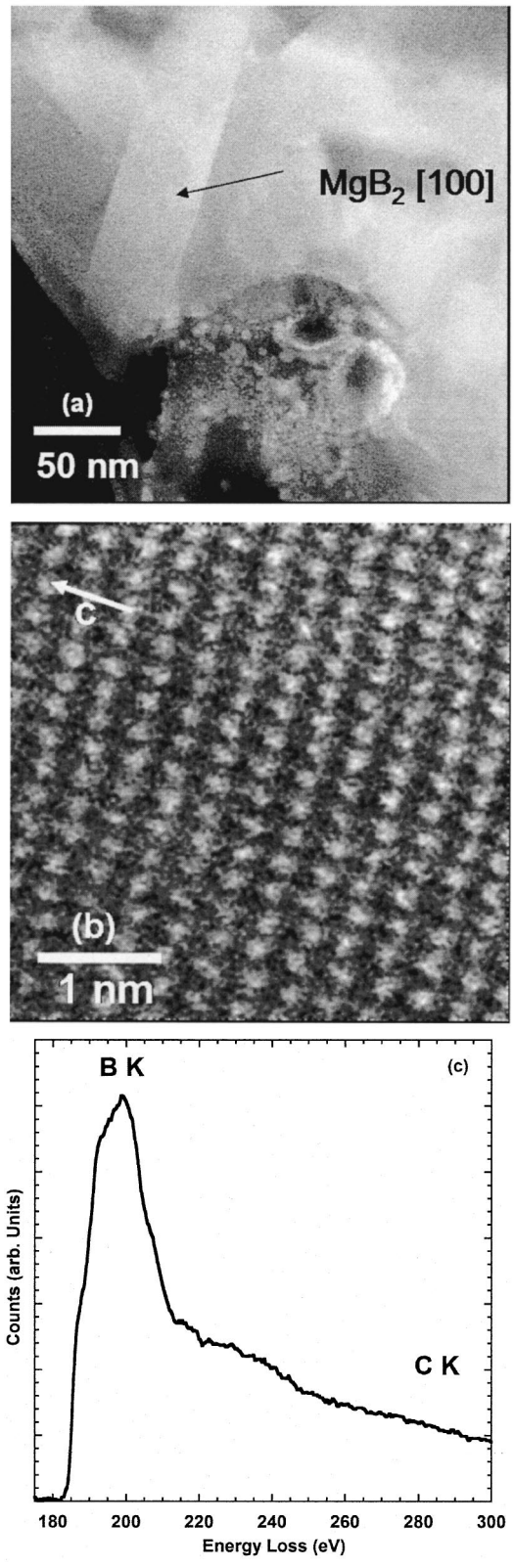

FIG. 8. (a) The *Z*-contrast image of a typical MgB_2 grain in the [100] orientation, (b) high-resolution *Z*-contrast image of the bulk of the MgB_2 grain showing the Mg columns only, and (c) EELS spectrum of the B K edge from the MgB_2 grain.

here that light elements, such as C or B, can be detected in concentrations down to 0.2% with a 10% accuracy in a matrix such as MgB_2. However, it is rather difficult to distinguish a small C signal originating from within the lattice or from surface contamination, as the low signal-to-noise ratio of the C core loss for such low concentrations makes it nearly impossible to distinguish the near-edge fine structure. Due to the large variety of phases present in the SiC-doped sample, it is therefore possible that C substitution at a level of 1%–3%, which is believed to be quite reasonable in the framework of the literature on C substitution,[15–19] cannot be readily identified, and more careful analysis is needed.

In addition to the high concentration of the nanoinclusions, there were structural defects observed in the nano-SiC-doped sample, as reported previously.[21] The majority of nanodomains have a rectangular shape with a domain size of about 2–4 nm. The domain boundaries trap numerous defects to form nanodefect wells and release the strain caused by the rotation of nanodomains, as reported by Li *et al.*[21] This nanodomain structure may be the result of a small proportion of C substituted for B. In our recent work, we found that C substitution indeed improved flux pinning while also depressing T_c. It was found that an optimal combination of substitution and addition achieved the best enhancement of flux pinning.[22]

DISCUSSION

In comparison to all other doping reported so far, the special features of nanoscale-SiC doping into MgB_2 can be described as follows: (1) the extent of enhancement in $J_c(H)$ is very large, by more than an order of magnitude above certain fields, (2) the enhancement of $J_c(H)$ extends to all temperatures up to T_c, in contrast to most of the other doping studies, which only show that it is effective in enhancing $J_c(H)$ at low temperatures, (3) although the value of H_{c2} for the SiC-doped sample is not as high as for the Mg-vapor-treated sample in the field range measured (Fig. 2), the $J_c(H)$ values for the SiC-doped sample are substantially higher than those of the Mg-vapor-treated sample, in particular, at higher temperatures (Fig. 4). These special features of the SiC-doped samples can be explained in terms of impurity scattering in the framework of two-gap superconductivity theory[3] and the improvement of flux pinning.

Role of impurity scattering

Recently, Gurevich *et al.*[3] reported a record-high $H_{c2}(0)=29$ T for untextured sample C and $H_{c2}^{\perp}(0)=34$ T and $H_{c2}^{\parallel}(0)=49$ T for a high-resistivity film [$\rho(40\text{ K})=220\ \mu\Omega$ cm] using direct, high-field resistivity measurements. In this study, a clean film with a low resistivity of 7 $\mu\Omega$ cm at 40 K had an $H_{c2}^{\parallel}$ of 29 T, in comparison to the 49 T of the 220 $\mu\Omega$ cm film. It seems likely that the SiC-doped sample with the highest resistivity of 300 $\mu\Omega$ cm will also have a very high H_{c2}.

To understand the significant enhancement of J_c at higher fields for the nano-SiC doping, we measured the resistivity ρ and residual resistivity ratio RRR for samples A and B, as shown from the resistivity versus temperature curves reported in Fig. 1. For comparison we list some literature data in Table I. The highest value of H^*_M correlates

TABLE I. Comparison of T_c, resistivity, and irreversibility field data for samples A, B, C, D, and one literature sample (pure sintered pellet made from ^{10}B).[23]

	Sample A: Undoped	Sample B: SiC doped	Sample C: Clean limit	Sample D: Mg vapor treated	Pure bulk
T_c (K)	37.2	36.5	39	36.9	40.2
ρ ($\mu\Omega$ cm) at 40 K	90	300	1	18	1
RRR	2.1	1.74	14.7	3	19.7
R(300 K)/R(40 K)					
H_M^* (20 K) (T)	5.6	7.4	3.9	5.2	3.8

well to the highest value of resistivity, both being found in the SiC-doped sample for which the $J_c(H)$ characteristics are best, too.

For the sample D, the Mg vapor treatment caused the increase in resistivity from 1 $\mu\Omega$ cm for the clean-limit sample C to 18 $\mu\Omega$ cm for sample D. Because Mg vapor treatment will largely affect the Mg sites in the lattice, the disorder in Mg sites will induce *out-of plane* π-band scattering which will increase the resistivity and dH_{c2}/dT at low temperatures and hence the H_{c2} at low temperatures. This was indeed confirmed later by the resistivity measurements in high field, which gave the value of H_{c2} (0) as about 29 T.[3] Sample D in Table I was measured after aging for two months, during which time the resistivity ρ dropped from its original value of 18−5 $\mu\Omega$ cm at 40 K, while T_c also increased from 36.9 to 37.7 K, due probably to relaxation of a quenched defect structure. As the Mg vapor treatment is unlikely to introduce impurities at grain boundaries, the increase in resistivity in this case can be considered to be tied to the improvement of H_{c2}. The improvement of H_{c2} at low temperatures leads to the improvement in $J_c(H)$ at low temperatures, as shown from the J_c versus H for sample D at 4.2 K in Fig. 4(a). The J_c of sample D is substantially larger than that of the clean-limit sample C and also crosses over sample A in higher fields.

As for sample B, according to the two-gap superconductivity theory,[3] the nano-SiC doping could lead to two different scattering channels. First, the partial C substitution for B sites causes disorder on the B sites which will result in in-plane σ scattering. The higher H_{c2} at higher temperatures contributes to the enhancement of $J_c(H)$ at higher temperatures for the SiC-doped sample. Second, the formation of nanodomain structures is due to the variation of Mg–B spacing which in turn causes disorder at B and Mg sites. These nanodomains with a size of 2−3 nm are also well below the 8−10-nm coherence length of MgB_2. These extensive nanodomain defects could result in strong in-plane and out-of-plane scattering and contribute to the increase of resistivity and H_{c2} in a wide temperature regime. This accounts for the enhancement of $J_c(H)$ in over a wide temperature range for the SiC-doped sample. Recently, a record-high H_{c2} (0) value of 37 T for bulk MgB_2 was achieved from transport measurements on a nano-SiC-doped sample, as reported by Serquis.[24] The strong upturn of $H_{c2}(T)$ at low temperatures indicates impurity scattering on the Mg sites.

Role of flux pinning

It should be pointed out that the resistivity of sample B (300 $\mu\Omega$ cm) is much larger than that of sample D (18 $\mu\Omega$ cm), although sample D has higher H_{c2} than sample B at least in the field region up to 9 T. In fact, the resistivity for the undoped sample A is already larger than sample D by a factor of 5, although the H_{c2} for A is much lower than for D. The large difference in resistivity between the Wollongong samples (A and B) and the Madison samples (C and D) is attributable to the different processing parameters used.[25] Samples C and D were prepared at 950−960 °C for 24 h in a highly protected environment (closed in a Ta or Nb tube and then sealed in a quartz tube), while samples A and B were processed at 800 °C for only 30 min in a sealed Fe tube, which cannot prevent oxygen diffusion through to the sample. As a result, samples C and D are of high quality, have large grains, and are free from impurities, as indicated by XRD,[4] while sample A has more impurities such as MgO which can be seen in the XRD pattern.[2] For sample B, the 10 wt % SiC addition into the sample A resulted in a further increase in the concentration of impurities through the reaction of SiC with Mg and B, including $MgSi_2$, BC, BO_x, $SiBO_x$, and unreacted SiC as identified by EELS and XRD. The resistivity of samples A and B may be strongly affected by the extrinsic mechanisms, such as scattering on the grain boundaries or second phase inclusions, which do not contribute to the enhancement of H_{c2} but certainly increases the global resistivity.

On the other hand, the additional impurities at nanoscale introduced by SiC doping can serve as strong pinning centers to improve flux pinning within a certain field region. This is clearly demonstrated by the superior J_c–H performance of the SiC-doped sample B, as shown in Figs. 3 and 4. It is particularly interesting to note that in Fig. 4(b), the J_c for B is higher than for D by a factor of as large as 100 at 20 K and 5 T even though the H_{c2} for D is higher than for B. This is further confirmed by the higher irreversibility line for B than for D, as shown in Fig. 5. The potential pinning centers introduced by SiC doping include inclusions, such as highly dispersed $MgSi_2$, BC, BO_x, and $SiBO_x$, which are all at a scale below 10 nm, match the coherence length very well and can act as strong pinning centers. Some large impurity particles such as unreacted SiC, as shown in Fig. 6(a), would not be effective pinning centers but act to reduce the superconducting volume and thus should be eliminated in order to further improve the zero-field J_c. In addition, the extensive network of nanodomain defects at a scale of 2−3 nm would

provide very effective collective pinning at all the temperatures up to T_c. All these defects are absent in sample D as Mg vapor treatment would not introduce these impurities. Thus, the flux pinning in sample D is not as strong as in sample B, at least at higher temperatures. At lower temperatures, the strong intrinsic scattering induced by Mg vapor treatment significantly enhances the H_{c2} which will, in turn, improve H_M^* and J_c at low temperatures for sample D. The fact that sample D has higher H_{c2} but lower H_M^* than sample B indicates that there are two closely related but distinguishable mechanisms that control the $J_c(H)$ characteristics: H_{c2} and flux pinning. The H_{c2} is the primary factor that sets the upper limit to H_M^* while the flux pinning is important to bring H_M^* closer to H_{c2} and improve the $J_c(H)$ within certain field regimes. These results suggest that we can manipulate the processing parameters that could lead to the improvement of either H_{c2} or flux pinning or of both at the same time. Recently, Matsumoto *et al.* reported that their Fe-sheathed SiC-doped MgB_2 wire achieved an H_M^* value of 23 T at 4.2 K by transport measurements,[25] which is consistent with the results we obtained previously[26] but extends them to higher fields. This is comparable to the conventional metallic superconductor, Nb_3Sn. The high value of H_M^* suggests that H_{c2} (0) for the SiC-doped sample would be greater than that for sample D (29 T).[3] This confirms that there are two mechanisms that are responsible to the significant enhancement of $J_c(H)$ performance in all the fields and temperatures: increase of H_{c2} and improvement of flux pinning in the SiC-doped sample.

CONCLUSION

In the framework of two-gap superconductivity, we have studied a set of four samples with very different resistivity and J_c characteristics as a result of different processing parameters and SiC doping. We have demonstrated that there are two closely related but distinguishable mechanisms that control the performance of $J_c(H)$: H_{c2} and flux pinning. Mg exposure to the clean-limit sample causes disorder on Mg sites whose scattering leads to the enhancement of H_{c2}. Nanoscale SiC doping into MgB_2 enhances both H_{c2} and flux pinning through multiple-scattering channels. Alloying at B and Mg sites due to C substitution and the formation of nanodomain structures causes strong scattering over a wide range of temperatures, leading to enhancement in H_{c2}. A high concentration of various nanoscale impurity phases results in high resistivity, a low residual resistivity ratio, and a large irreversibility field and upper critical field with modest T_c reduction. The highly dispersed nanoscale precipitates $MgSi_2$, BC, BO_x, and $SiBO_x$ and the extensive domain structures at a scale well below 10 nm serve as strong pinning centres. Doping with SiC enhances the critical current density, the irreversibility field, and the upper critical field in a manner that helps make MgB_2 potentially competitive with both low- and high-T_c superconductors.

ACKNOWLEDGMENTS

The authors thank J. Horvat, M. J. Qin, A. Pan, M. Ionescu, T. Silver, H. K. Liu, M. Tomsic, and E. W. Collings for their help in various aspects of this work. The work in Wollongong was supported by the Australian Research Council, Hyper Tech Research Inc., OH, USA, Alphatech International Ltd., NZ, and the University of Wollongong, while that in Madison was supported by NSF through the MRSEC on Nanostructured Materials and Interfaces.

[1] J. Nagamatsu, N. Nakagawa, T. Muranaka, Y. Zenitani, and J. Akimitsu, Nature (London) **410**, 63 (2001).
[2] S. X. Dou, S. Soltanian, X. L. Wang, P. Munroe, S. H. Zhou, M. Ionescu, H. K. Liu, and M. Tomsic, Appl. Phys. Lett. **81**, 3419 (2002).
[3] A. Gurevich *et al.* Supercond. Sci. Technol. **17**, 278 (2003).
[4] V. Braccini, L. D. Cooley, S. Patnaik, D. C. Larbalestier, P. Manfrinetti, A. A. Palenzona, and A. S. Siri, Appl. Phys. Lett. **81**, 4577 (2002).
[5] J. Horvat, S. Soltanian, X. L. Wang, and S. X. Dou, Appl. Phys. Lett. **84**, 3109 (2004).
[6] J. E. J. E. Evetts, *Concise Encyclopedia of Magnetic and Superconducting Materials* (Pergamon, New York, 1992), p. 99.
[7] R. F. Egerton, *Electron Energy Loss Spectroscopy in the Electron Microscope* (Plenum, New York, 1986).
[8] R. A. Ribeiro, S. Budko, C. Petrovic, and P. C. Canfield, Physica C **384**, 227 (2003).
[9] R. Flukiger, H. L. Suo, N. Mugolino, C. Benedice, P. Toulemonde, and P. Lezza, Physica C **385**, 286 (2003).
[10] S. X. Dou, A. V. Pan, S. Zhou, M. Ionescu, H. K. Liu, and P. R. Munroe, Supercond. Sci. Technol. **15**, 1 (2002).
[11] C. B. Eom *et al.* Nature (London) **411**, 558 (2001).
[12] S. M. Kazakov, J. Karpinski, J. Jun, P. Geiser, N. D. Zhigadlo, P. Puznak, and A. V. Mironov, e-print cond-mat/0304656.
[13] T. Takenobu, T. Ito, D. H. Chi, K. Prassides, and Y. Iwasa, Phys. Rev. B **64**, 134513 (2001).
[14] I. Maurin, S. Margadonna, K. Prassides, T. Takenobu, Y. Iwasa, and A. N. Fitch, Chem. Mater. **14**, 3894 (2002).
[15] W. Mickelson, J. Cumings, W. Q. Han, and A. Zettl, Phys. Rev. B **65**, 052505 (2002).
[16] Z. H. Cheng, B. G. Shen, J. Zhang, S. Y. Zhang, T. Y. Zhao, and H. W. Zhao, J. Appl. Phys. **91**, 7125 (2002).
[17] E. M. James and N. D. Browning, Ultramicroscopy **78**, 125 (1999).
[18] N. D. Browning, M. F. Chrisholm, and S. J. Pennycook, Nature (London) **366**, 143 (1993).
[19] G. Duscher, N. D. Browning, and S. J. Pennycook, Phys. Status Solidi A **166**, 327 (1998).
[20] R. F. Klie, J. C. Idrobo, N. D. Browning, K. A. Regan, N. S. Rogado, and R. J. Cava, Appl. Phys. Lett. **79**, 837 (2001).
[21] S. Li *et al.* Appl. Phys. Lett. **83**, 314 (2003).
[22] S. X. Dou, W. K. Yeoh, J. Horvat, and M. Ionescu, Appl. Phys. Lett. **83**, 4996 (2003).
[23] D. K. Finnemore, J. E. Ostenson, S. L. Bud'ko, G. Lapertot, and P. C. Canfield, Phys. Rev. Lett. **86**, 2420 (2001).
[24] A. Serquis, Presented at the Fall Meeting of MRS, Boston, MA, 1–5 December 2003.
[25] A. Matsumoto, H. Kumakura, H. Kitaguchi, and H. Katakeyama, Supercond. Sci. Technol. **16**, 926 (2003).
[26] S. X. Dou, J. Horvat, S. Soltanian, X. L. Wang, M. J. Qin, S. H. Zhou, H. K. Liu, and P. G. Munroe, IEEE Trans. Appl. Supercond. **13**, 3199 (2003).